Hindawi
Journal of Food Quality
Volume 2021, Article ID 4497128, 14 pages
https://doi.org/10.1155/2021/4497128

Research Article

Preparation and Characterization of *Auricularia cornea Ehrenb* Polysaccharide-Zn Complex and Its Hypoglycemic Activity through Regulating Insulin Resistance in HepG2 Cells

Tingting Liu,[1,2] **Shanshan Zhang**,[1,2] **Nan Wang**,[1,3] **Xinle Xu**,[1,2] **Hongcheng Liu**,[1,2] **Dawei Wang**,[1,2] **and Yanrong Zhang**[1,4]

[1]*School of Food Science and Engineering, Jilin Agricultural University, Changchun 130118, China*
[2]*Engineering Research Center of Grain Deep-processing and High-effeciency Utilization of Jilin Province, Changchun 130118, China*
[3]*Key Laboratory of Technological Innovations for Grain Deep-processing and High-effeciency Utilization of By-products of Jilin Province, Changchun 130118, China*
[4]*Scientific Research Base of Edible Mushroom Processing Technology Integration of Ministry of Agriculture and Rural Affairs, Changchun 130118, China*

Correspondence should be addressed to Yanrong Zhang; zhangyanrong0044@jlau.edu.cn

Received 5 August 2021; Accepted 26 October 2021; Published 10 December 2021

Academic Editor: Changyang Ma

With *Auricularia cornea Ehrenb* polysaccharide (ACEP) as raw material, the purpose of the study was to prepare *Auricularia cornea Ehrenb* polysaccharide-zinc (ACEP-Zn) complex. Fourier transform infrared spectroscopy (FT-IR), X-ray diffraction (XRD), scanning electron microscopy (SEM), nuclear magnetic resonance (NMR), and other means are used to analyze the physical-chemical properties and structure of ACEP and ACEP-Zn, to investigate the inhibition of α-glycosidase and α-amylase enzymes, and to explore its effects on the glucose metabolism of insulin-resistant HepG2 cells. Nuclear magnetic resonance (NMR) results show that a group of COO-, -CH3, and -OH in the sugar chain binds to Zn^{2+}. Compared with the original polysaccharides, the surface morphology of ACEP-Zn changed obviously, and the molecular weight (Mn) of ACEP-Zn decreased, but the molecular agglomeration of ACEP-Zn increased. Moreover, the inhibitory effect of ACEP-Zn on α-glucosidase and α-amylase was stronger than that of the original polysaccharide. The results indicated that the structure of *Auricularia cornea Ehrenb* polysaccharide was changed obviously after the zinc complex, and its hypoglycemic activity was enhanced in vitro. In the cell experiment, the glucose consumption of IR-HepG2 cells was significantly increased at a concentration of 50–200 μg/mL ($P < 0.05$). The activity of SOD and NOS significantly increased ($P < 0.01$), and the activity of intracellular PK increased ($P < 0.05$). Therefore, it was speculated that the hypoglycemic effect of *Auricularia cornea Ehrenb* polysaccharide combined with zinc was related to the alleviation of liver cell damage caused by oxidative stress and the improvement of glucose metabolism of IR-HepG2 cells. The study provides a theoretical basis for the application of the polysaccharide-zinc complex in the hypoglycemic functional food field.

1. Introduction

Type 2 diabetes mellitus (T2DM), an epidemic metabolic disease characterized by postprandial hyperglycemia, has become a major global health problem, which is predicted to affect approximately 439 million people by 2030 [1, 2]. Due to the decline in glucose uptake and metabolism in various organs, the blood and liver glucose and lipids are abnormally increased, resulting in hyperglycemia, hypertension and hyperlipidemia, central obesity, atherosclerosis, and other risk diseases [3]. Insulin resistance (IR) will trigger compensatory secretion of insulin, load of pancreatic islet cells, and function failure, thus making people with metabolic disorders develop into T2DM patients [4]. The liver, as the

key organ of glucose and lipid metabolism in the human body, plays a special role in systemic insulin sensitivity [5]. Current treatments for T2DM include insulin and its analogues, sulfonylureas, thiazolidinediones, exenatide, and biguanide [6]. However, these interventions and oral drugs have the potential to have adverse effects, which are expensive. Therefore, it is necessary to explore new functional foods or drugs to prevent the occurrence of T2DM, improve the therapeutic effect of T2DM, and reduce its complications.

Zinc (Zn), one of the essential trace elements in the human body, is a component or activator of many enzymes [6]. It plays an important role in maintaining normal physiological function, enhancing immunity, and promoting the physical and intellectual development of the human body [7]. Studies have reported that zinc could lower the blood sugar level of mice and correct impaired glucose tolerance [8]. When the mice were deficient in zinc, they were resistant to exogenous insulin, and their glucose metabolism ability was decreased [9]. In cell experiments, Zn stimulated glucose uptake in adipocytes, induced phosphorylation of AKT and GSK3B in 3T3-L1 fibroblasts, and induced GLUT4 transfer to the cell membrane [10, 11]. With the development of research, the role of Zn in the occurrence and development of diabetes has gradually been clarified, and the supplementary therapy of Zn has a significant effect on diabetic animals and diabetic patients, suggesting that this metal may become a new measure of diabetes treatment in the future. However, most Zn supplement products are mostly inorganic Zn, which is not conducive to human absorption and is toxic. The characteristics of organic Zn are easy absorption, low toxicity, and higher biological functions. Inorganic Zn can be changed into organic Zn by some biological means [12]. Recent studies have shown that the application of ligand-Zn is the main way, which improves the biological activity of Zn and reduces its toxicity [13, 14]. Due to their good biocompatibility, such as stability, good biodegradability, and multiple biological activities, polysaccharides can be used as excellent Zn complexes. In recent years, people have prepared some polysaccharide Zn complexes and evaluated their biological activities. Wang Pingping et al. found that the antioxidant and hypoglycemic activities of *Fructus mori* polysaccharide-zinc were higher than polysaccharide at the same concentration [15]. At present, the reported polysaccharide-Zn complex includes *Thunb* polysaccharide-zinc [10], *Prunella vulgaris* L. polysaccharide-zinc [11], and *Dictyophora indusiata* polysaccharide-zinc [12].

Auricularia cornea Ehrenb (ACE) is a genus of jelly fungi in the family Auriculariaceae, and belongs to a variant of *Auricularia cornea* species. ACE has nutritional value and medical applications, which were first reported and cultured by the research team led by Prof. Li (the Chinese Academy of Engineering) at Jilin Agricultural University, Jilin, China [15, 16]. With high protein and low fat, it can avoid gaining weight after eating. Long-term use is beneficial to health, and dietary fiber can promote gastrointestinal motility, digestion, and absorption. It has been reported that *ACE* has antidiabetes and antinephritis effects, and it was speculated that the polysaccharide of *Auricularia cornea Ehrenb* (ACEP) might be the main reason of these beneficial effects [17, 18]. ACEP can play an important role in lowering blood sugar and blood lipid levels, antioxidation, and anticancer.

The aim of this study was to obtain ACEP-Zn and clarify its structural characterization. By inhibiting α -glucoside and α -amylase activities, an insulin-resistant HepG2 cell model (IR-HepG2) was established to evaluate the hypoglycemic activity of CMP2B. The regulatory effect of ACEP-Zn on insulin resistance was investigated by detecting glucose consumption, oxidative stress response SOD and NOS, and glycolytic rate-limiting enzyme PK activity in IR-HepG2 cells. The aim of this work was also to reveal the preliminary hypoglycemic mechanism of ACEP-Zn. This study will not only help to promote the efficient utilization of edible mushrooms such as *Auricularia cornea Ehrenb* and follow the concept of "Small Auricularia, big industry" but also develop a potential new organic Zn supplement to prevent the occurrence of T2DM.

2. Materials and Methods

2.1. Materials. *Auricularia cornea Ehrenb* was made by the academician from Li Yu Laboratory of edible fungus processing, Jilin Agricultural University. The $ZnSO_4$ with analytical grade was purchased from the Aladdin Chemistry Company (Shanghai, China). Dimethyl sulfoxide (DMSO), 3-(4,5-dimethyl-2-thiazolyl)-2,5-diphenyl tetrazolium bromide (MTT), p-nitrophenyl-β-D-galactopyranoside (pNPG), fetal bovine serum (FBS), phosphate-buffered saline (PBS), α-glucosidase, and α-amylase were purchased from Sigma-Aldrich Chemical Co. (St. Louis, MO, USA). HepG2 cells were purchased in Jilin province from Beijing Biological Company. The glucose assay, pyruvate kinase (PK), superoxide dismutase (SOD), and total nitric oxide synthase (NOS) kits came from the Nanjing Jiancheng Bioengineering Institute (Nanjing, China). All of the other chemicals used in this experiment were analytical grade.

2.2. Preparation of ACEP. ACEP was prepared according to our previous study [19]. In brief, crude polysaccharides were extracted from *Auricularia cornea Ehrenb* using enzymatic hydrolysis and pressurized hot water. 10 g of 140-mesh auricula powder was accurately weighed, distilled water was added, and 1.0% cellulase was added according to the solid-liquid ratio of 1 : 100 (g/mL), pH = 5.0, extraction at 50°C for 120 min, and inactivation at 100°C for 15 min. The sample solutions after enzymation were put into a high-pressure reaction kettle for extraction at 100°C. The pressure was 2.0 MPa, the reaction time was 55 min, and then sequentially fractionated and purified using DEAE-52 cellulose and Sephadex G-100 to obtain the polysaccharide ACEP.

2.3. Preparation of ACEP-Zn. The ACEP (1.0 g) was mixed in 100 mL of distilled water and stirred for 15 min at 55°C. After adding 0.6 g of $ZnSO_4$ (0.1 mol/L H_2SO_4) and mixing, 1 mol/L NaOH was used to adjust appropriate pH = 6 at 50°C,

reaction for 2.0 h. At the end of the reaction, it was centrifuged (5000 rpm, 10 min) to remove the undissolved substances. The precipitate appeared by adding a four-fold amount of ethanol and was kept overnight at 4°C. After centrifugation again, the precipitate was dissolved in water and then freeze-dried to obtain ACEP-Zn powder. The Zn content was tested by a graphite furnace atomic absorption spectrometer (AAS) (Z-5000, Hitachi, Japan).

2.4. Structural Characterization of ACEP and ACEP-Zn

2.4.1. Molecular Weight Determination. A 2.0 mg/mL ACEP and ACEP-Zn solution (2.0 mg/mL) were filtered through a 0.45 μm membrane and then injected into a high-performance gel permeation chromatography (HPGPC) machine (1515, Waters, USA) [17]. Test conditions were as follows: 1515 high-performance liquid chromatography; ultrahydrogel 500, 2000 chromatographic column; 2414 differential refractive detector; mobile phase was 0.1 mol/L $NaNO_3$ solution; and the flow rate was 0.5 mL/min. The temperature of the column and detector was 35°C, and the sample volume was 25 μL.

2.4.2. FT-IR Spectroscopy. The FT-IR spectral analyses of ACEP and ACEP-Zn were performed by a Nicolet iS20 FT-IR spectrophotometer (Thermo Fisher Inc., USA) and recorded at 400–4000 cm^{-1}.

2.4.3. Scanning Electron Microscopy (SEM). The dried powder of samples was placed on tapes, sputtered with gold, and determined by SEM with an acceleration voltage of 5 kV. SEM images of ACEP and ACEP-Zn samples were obtained by an environmental scanning electron microscope (JSM-7500F, JEOL, Japan).

2.4.4. XRD Analysis. The structural states of ACEP-5 and ACEP-5-Zn were studied by XRD (Advance, Bruker, Germany). The XRD conditions were as follows: 40 kV, 40 mA, Cu target, 0.02° minimum step size, 0–90° scanning angle, and 4.0°/min scanning rate.

2.4.5. DSC Analysis. DSC analysis was performed on a differential scanning calorimetry instrument (DSC25, TA, USA). Samples were recorded at the range of 20–400°C under nitrogen atmosphere (99.9%) with a heating rate of 10°C/min. The sample pool was an aluminum crucible.

2.4.6. Nuclear Magnetic Resonance (NMR) Spectroscopy. The ACEP and ACEP-Zn samples (60 mg) were fully dissolved in D_2O (0.5 mL) at room temperature in an NMR tube. ^{13}C and ^{1}H NMR spectra were analyzed by a Bruker 600 MHz NMR spectrometer (Bruker, Fallanden, Switzerland).

2.5. Hypoglycemic Activity In Vitro

2.5.1. Inhibitory Activities against α-Glucosidase. The α-glucosidase inhibitory activity was performed by the previously reported method with some modifications [20]. ACEP and its Zn complex were prepared into sample solutions at concentrations of 5, 10, 15, 20, and 25 mg/mL, respectively. 5 mmol/L of pNPG and 0.1 U/mL of α-glucosidase solutions were prepared with 100 mmol/L of PBS (PH 6.8), respectively. 50 μL of sample solution to be tested was transferred into 96-well plate, and 50 μL of pNPG solution was added to each of them, incubated at 37°C for 10 min. Then, 50 μL of α-glucosidase solution was added to each of them and placed in the microplate analyzer for reaction at 37°C for 30 min. The absorbance A was measured at a wavelength of 405 nm. The following equation was used to calculate the inhibition rate:

$$\mathrm{IR} = \left(1 - \frac{(A_1 - A_2)}{A_0 - A_3}\right) \times 100\%, \quad (1)$$

where A_1 was the absorbance of the sample group; A_0 was the absorbance of the blank group; A_2 was the absorbance of PBS instead of α-glucosidase solution; and A_3 was the absorbance of ACEP and α-glucosidase solution replaced by distilled water and PBS, respectively.

2.5.2. Inhibitory Activities against α-Amylase. The α-amylase inhibitory activity was used the method of Adefegha et al. [21] with minor modifications. ACEP and Zn complex were prepared into sample solutions at concentrations of 5, 10, 15, 20, and 25 mg/mL, respectively.10 U/mL α-amylase solution and 1% soluble starch solution were prepared with 25 mmol/L PBS (pH 6.9). In each tube, 300 μL of solution to be tested and α-amylase solution were added and incubated at 37°C for 15 min. 300 μL of soluble starch solution was added to start the reaction. After 15 min, 500 μL of DNS was added to each tube for color development. The reaction was terminated by boiling for 10 min immediately. The volume of the mixed system was fixed to 10 mL, and the absorbance was measured at 540 nm. The following equation (2) was used to calculate the inhibition rate:

$$\mathrm{IR} = \left(1 - \frac{(A_1 - A_2)}{A_0 - A_3}\right) \times 100\%, \quad (2)$$

where A_1 was the absorbance of the sample group; A_0 was the absorbance of the blank group; A_2 was the absorbance of replacing α-amylase solution with PBS; and A_3 was the absorbance of ACEP and α-amylase solution replaced by distilled water and PBS, respectively.

2.5.3. Effect of ACEP-Zn on HepG2 Cell Proliferation. The experiments related to the effect on HepG2 cell proliferation were performed to determine the security of ACEP-Zn.In brief, we selected the log-phase HepG2 cells, added 0.25% trypsin for digestion, adjusted the cell density, inoculated the 96-well plate, and cultured them in a 5% CO_2 incubator at 37°C for 12 h. After the HepG2 cells adhered to

the wall, 200 μL of complete culture medium was added to the blank group and 200 μL of ACEP-Zn solution (10, 25, 50, 100, 200, and 400 μg/mL) to the sample group. Continuing to culture for 24 hours, MTT solution (20 μL per well) was added. After 4 h of incubation, DMSO solution (150 μL per well) was added to terminate the reaction. The absorbance was tested at 490 nm.

2.5.4. Glucose Consumption Assay. The glucose consumption assay was performed by the previously reported method with some modifications [22]. In order to explore the effects of ACEP-Zn on glucose consumption, we modified the IR-HepG2 cell model based on the reported high glucose induction [23]. In short, HepG2 cells were simply cultured in 6-well plates at 37°C with 5% CO_2 until 70–90% of the cells were confluent. Incubation continued for 3 hours to ensure that the no-serum DMEM (high glucose) synchrony cells were used. After medium removing, fresh DMEM (high sugar) containing 1.0×10^{-6} mol/L insulin and 2% FBS was added to each group and left for 48 hours. Different concentrations of ACEP-Zn solutions (10, 25, 50, 100, 200, and 400 μg/mL) were used for intervention treatment and incubated with IR-HepG2 cells. The blank control was cells without insulin treatment, and the model control was treated with phosphate buffer (nonsample). The concentrations of glucose in the supernatant were determined by the glucose assay kit purchased from Nanjing Jiancheng Bioengineering Institute (Nanjing, China).

2.5.5. Determination of Activities of SOD, NOS, and PK. Making relevant modifications according to previous studies [24]. HepG2 cells (1×10^4 cells/mL, 0.1 mL) were inoculated in 96-well plates and incubated in 5% CO_2 at 37°C for 24 h. Then, the culture medium was removed and the cells were washed twice with PBS. IR-HepG2 cell model was established by adding 1.0×10^{-6} insulin (3 mol/L) and 2% FBS to fresh DMEM (high glucose) for 48h in each group. Then, the experiments were carried out with the blank group (no cells), the normal group (with HepG2 cells), the model group (with HepG2-IR cells), and the experimental group (with IR-HepG2 cells and ACEP-Zn (10, 25, 50, 100, 200, and 400 μg/mL)). The concentrations of ACEP-Zn were (10, 25, 50, 100, 200, and 400 μg/mL) After 24 h, the activities of NOS, SOD, and PK were measured with the instructions of kits (Nanjing Jiancheng, China).

2.6. Statistical Analysis. All experiments were expressed as mean standard deviation (SD) ± for the three measurement methods. The statistical significance of the difference values were recorded in $P < 0.05$ or $P < 0.01$. All statistical analyses were evaluated using existing statistical software (SPSS20.0, L, USA).

3. Results and Discussion

3.1. Synthesis of ACEP-Zn Complex. The theory of atomic absorption spectrometry (AAS) is based on the atomic absorbance, which corresponds to the signal generated by the measured atomic weight being measured and is sufficiently sensitive to measure the trace metals in the sample [25]. In the study, ACEP-Zn was successfully synthesized by the reaction of polysaccharide ACEP with $ZnSO_4$. The zinc content of the ACEP-Zn complex was 5.41 ± 0.01 mg/g. The ACEP-Zn complex was synthesized under the optimum conditions: the ratio of ACEP and $ZnSO_4$ was 10 : 8 (w/w), the pH was 5, the reaction temperature was 50°C, and the reaction time was 2.5 h.

3.2. Molecular Weight Determination. As could be seen from Figure 1, the HPGPC chromatographic peaks of ACEP and ACEP-Zn showed a single peak shape, indicating that both of them are composed of uniform components. It could be seen from Table 1 that the average molecular weight (M_W) of ACEP was 35,479 g/mol, higher than that of ACEP-Zn (32,667 g/mol). The results indicated that the molecular weight of ACEP-Zn decreased significantly after the Zn complex reaction, which might be attributed to the use of dilute hydrochloric acid to regulate pH value during the complex reaction. As hydrochloric acid is a strong acid, part of the polysaccharide degrades, and some of its active groups are exposed, thus enhancing its biological activity. The results were similar to those obtained by Wei et al. [26]. Through the establishment of a HepG2 cell insulin resistance model, Wang et al. explored the mechanism of hypoglycemic activity of the mulberry polysaccharide Zn complex. Both results showed that compared with the original polysaccharide, mulberry polysaccharide Zn had stronger activity of fall blood sugar, and it could promote more insulin secretion and relieve more insulin resistance [27]. The reason was that the molecular weight of ACEP-Zn was smaller than that of ACEP, and the substances with smaller molecular weight are easier to act in cells through the membrane, so its hypoglycemic activity ACEP-Zn stronger than that of ACEP, which may be one of the reasons why the hypoglycemic activity of ACEP-Zn was stronger than that of ACEP, which needed to be further explored and studied.

3.3. FT-IR Spectrometric Analysis. The FT-IR spectrums of ACEP and ACEP-Zn are shown in Figure 2. The wide peak of ACEP at 3380 cm^{-1} was due to the stretch vibration of -OH bond, and the absorption peak in ACEP-Zn was moved to 3360 cm^{-1}, indicating that the coordination reaction between –OH in ACEP and Zn^{2+} occurred [28]. This phenomenon was that the -OH groups of polysaccharides participated in the coordination of Zn^{2+}, formed intermolecular hydrogen bonds, and enhanced intermolecular interactions. The peak of ACEP at 2920 cm^{-1} was found to be the absorption peak of the -CH asymmetric stretching vibration in methyl (-CH_3). In ACEP-Zn, the absorption peak was moved to 2940 cm^{-1}, indicating that -CH_3 in ACEP had a coordination reaction with Zn^{2+}. The peak of ACEP at 1620 cm^{-1} was attributed to an asymmetric -C=O stretching vibration in the carboxy group (-COO^-). And the absorption peak in ACEP-Zn was moved to 1650 cm^{-1},

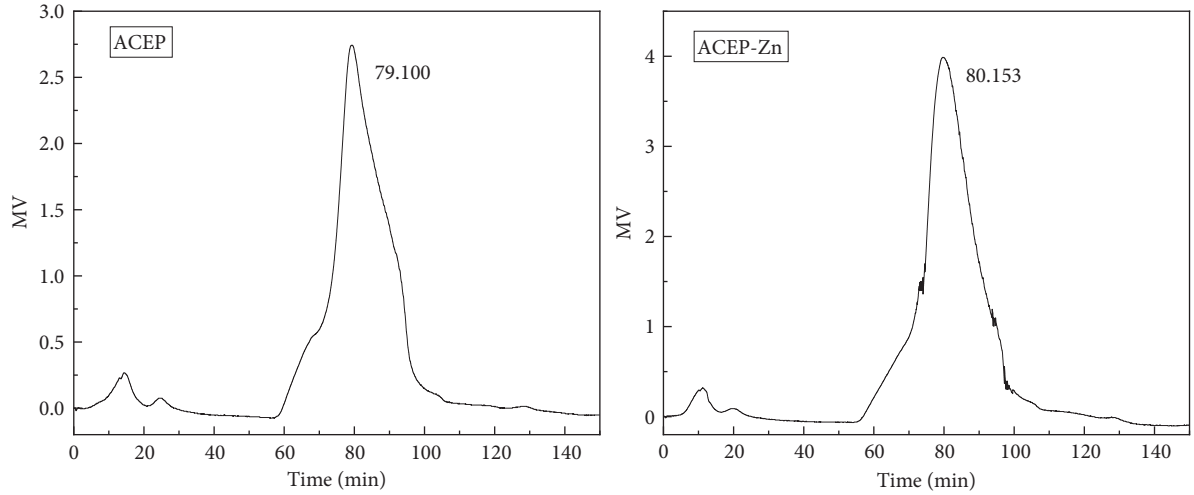

Figure 1: Molecular weight distribution of ACEP and ACEP-Zn.

Table 1: Molecular characteristic parameters of ACEP and ACEP-Zn complex.

Molecular characteristic parameter	ACEP	ACEP-Zn
M_n (g/mol)	21705	21310
M_w (g/mol)	35479	32667
M_w/M_n	1.635	1.533

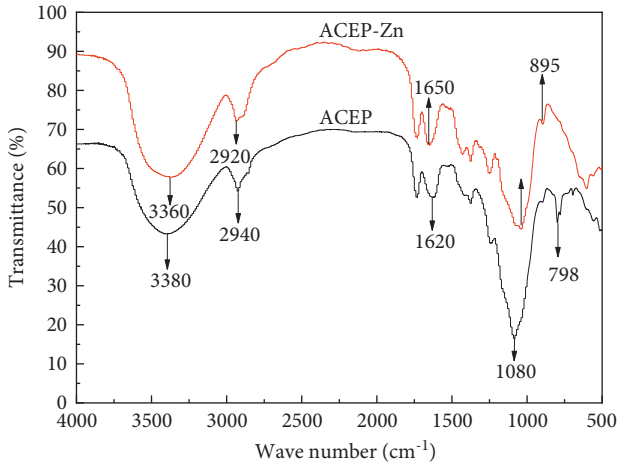

Figure 2: Fourier transform infrared spectroscopy (FT-IR) of ACEP and ACEP-Zn complex.

indicating -COO- groups might have participated in coordination with Zn^{2+} [29]. The absorption peaks of ACEP at 1240 cm^{-1} and 1080 cm^{-1} corresponded to the stretching vibration of the O-H and C-O-C groups, respectively. Moreover, the absorption peaks in ACEP-Zn were moved to 1250 cm^{-1} and 1040 cm^{-1}, respectively. Additionally, the absorption peaks at 798 cm^{-1} disappeared in ACEP. In summary, the coordination reaction of Zn^{2+} polysaccharide was mainly reflected in the reaction of -OH, $-CH_3$, -COO-, and other groups with Zn^{2+}, rather than simple physical mixing.

3.4. SEM Analysis. Scanning electron microscopy (SEM) was used to observe the surface morphological characteristics changes of ACEP before and after being chelated with Zn^{2+}. As shown in Figure 3, the SEM image of ACEP exhibited a smooth and tight surface, which was closely associated with its microscopic structure. By comparison, the morphologies of ACEP-Zn samples were substantially different from those of ACEP. However, the surface of ACEP-Zn was rough with many layers, which suggested that the Zn^{2+} successfully bridged the ACEP molecules and created their aggregations. Additionally, there were some small clastic particles on the surface. Therefore, it could be concluded that ACEP might have physical adsorption phenomena besides the complex reaction between ACEP and Zn.

3.5. DSC Analysis. In order to identify the thermal characteristics of the ACEP-Zn complex before and after the reaction and the thermal stability of the reaction products, ACEP and ACEP- Zn were analyzed by differential scanning calorimetry. As shown in Figure 4, both ACEP and ACEP-Zn had an obvious endothermic peak at 115°C, which might be due to the evaporation of water in sugar molecules and the absorption of heat. ACEP had an obvious endothermic peak at 255°C, which might be due to the heat absorbed by the redox reaction of hydroxyl and carbonyl groups in sugar molecules. ACEP-Zn had a new exothermic peak at 360°C, which indicated that the hydroxyl and carbonyl groups in sugar molecules did not undergo redox reaction, but coordinated reaction with Zn^{2+} to form a new polysaccharide Zn^{2+} compound. And the stability of ACEP was higher than that of ACEP-Zn.

3.6. XRD Analysis. The X-ray diffraction (XRD) profile of ACEP and ACEP-Zn complexes from 0° to 90° is exhibited in Figure 4. It could be seen that ACEP and its ACEP-Zn only in 20° had a diffraction peak, suggesting that ACEP and the ACEP-Zn complex were both amorphous substances.

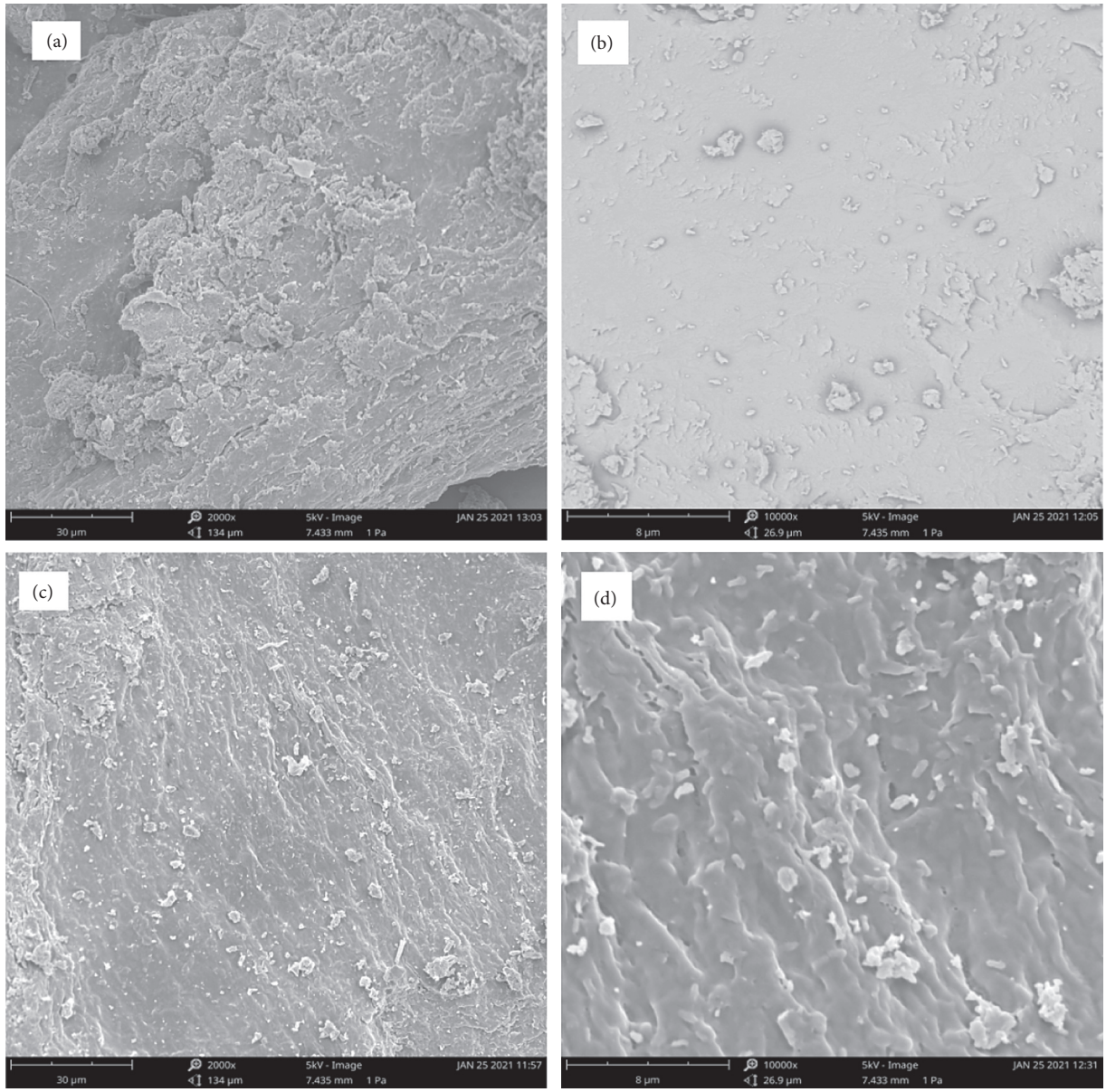

Figure 3: Morphological observation of ACEP and ACEP-Zn complex. (a, b) Scanning electron microscope (SEM) image of ACEP; (c, d) scanning electron microscope (SEM) image of ACEP-Zn complex.

The result was similar to the study of the chitosan-zinc complex [30]. As shown in Figure 5, the strength of the peak was higher than that of ACEP but did not find the characteristics of the Zn^{2+} sulfate diffraction peak, both for the amorphous structure, and once again proved that ACEP and Zn^{2+} did undergo complexation, which led to the speculation that Zn^{2+} could be evenly dispersed in ACEP on the chain of sugar and form a complex. The distribution of ACEP indicated that the overall crystallinity was low. The properties of ACEP were not affected by the combination of Zn^{2+}, indicating that the structure of ACEP was basically unchanged. The results were consistent with the report of Yun et al. [31] on the preparation of polysaccharides-Zn from rattan. This might be due to the complex chemical structure of polysaccharides, which are often composed of more than thousands of monosaccharides through glycosylic bonds. After chelating with Zn^{2+}, the amorphous properties of the polysaccharide did not change.

3.7. NMR Spectra Analysis. NMR spectroscopy can be used as an important means to further characterize the structural characteristics of AEPS and AEPS-Zn by analyzing the plasmid structure, linkage pattern, and a series of sugar units in the molecules [32]. NMR spectra were used to analyze the chemical shifts of main chain residues that occurred in the repeating units.^{1}HNMR spectra of ACEP and ACEP-Zn are shown in Figures $6(a)_1$ and $6(a)_2$. The^{1}HNMR spectrum signals of the two samples were mostly concentrated in the δ (3.0–5.0) PPM region. The very strong signal peak near δ4.79

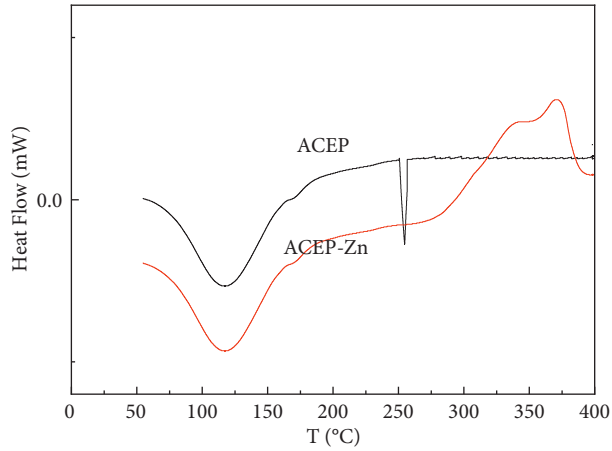

Figure 4: DSC picture of ACEP and ACEP-Zn complex.

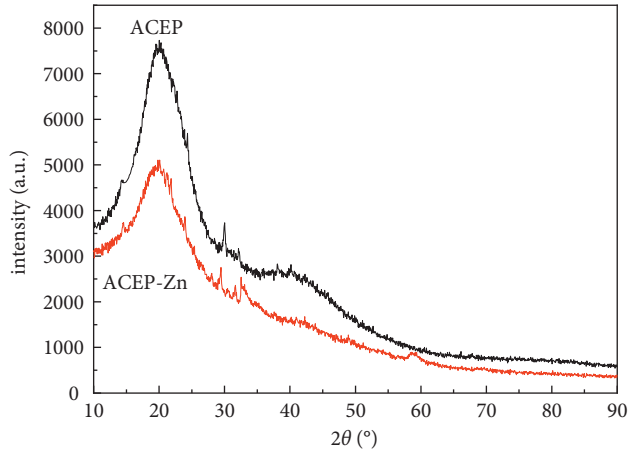

Figure 5: XRD patterns of ACEP and ACEP-Zn.

PPM was the formant of D_2O. Studies have shown that the proton chemical shift of β-type pyranose residues is below 5.0 ppm and that of α-type pyranose residues is above 5.0 ppm, which could distinguish the types of sugar rings [33]. In the heterocephalic hydrogen proton signal range, ACEP had three signals at 4.44, 4.51, and 4.54 ppm, indicating that it was a β-pyranose, which was consistent with the FT-IR analysis. Compared with the ^{1}HNMR spectra of ACEP, the H intensity of AEPS-Zn spectra was obviously weakened and the peak deformation was wider. ACEP-Zn also has four signals at 4.1, 4.21, 4.26 and 4.34 ppm, indicating that it was a β-pyranose. This was because when the ACEP ligand was integrated with zinc, the relaxation time of the ACEP ligand was shortened and the signal range was so wide that the signal around the paramagnetic Zn^{2+} could not be detected. Therefore, a blind region was formed centered on Zn^{2+} with high spin, which provided a basis for the occurrence of the integration reaction between ACEP and Zn.

The so-called ^{13}CNMR usually refers to the spectrum obtained by the full decoupling method, and the chemical shift of the carbon spectrum is concentrated around 0–200 ppm [34]. In polysaccharides, the signal of heterocarbonate is mostly distributed in the low field of 90–120 ppm, and the signal number in this region is related to the composition number of monosaccharides and the chemical shift is close to and easily overlaps [35]. The carbon spectra of ACEP and ACEP-Zn are shown in Figures $6(b)_1$ and $6(b)_2$. The carbon spectra of ACEP showed that there were three major signal peaks (96.11, 99.07, and 103.43 ppm) in the first carbon region of 90–120 ppm, indicating that ACEP mainly contained three sugar residues and β-pyranose glycogen bonds. This result was consistent with the ^{1}HNMR result of ACEP; compared with the ^{13}CNMR map of ACEP, the basic carbon skeleton of ACEP-Zn polysaccharides did not change. The signal peaks of ACEP and ACEP-Zn appeared at 172.96 ppm and 172.89 ppm, indicating that both of them were acidic polysaccharides. There was no proton chemical shift between 82 and 88 ppm, and both of them were pyranose. The main signal peak of ACEP-Zn appeared around 96–103, indicating that the C_1 polycephalic carbon in ACEP was replaced. A group of strong peaks appeared at 70–77 ppm, indicating that the signal peak formed by C_2, C_3, C_4, or C_5 was not replaced, and 69.27 ppm

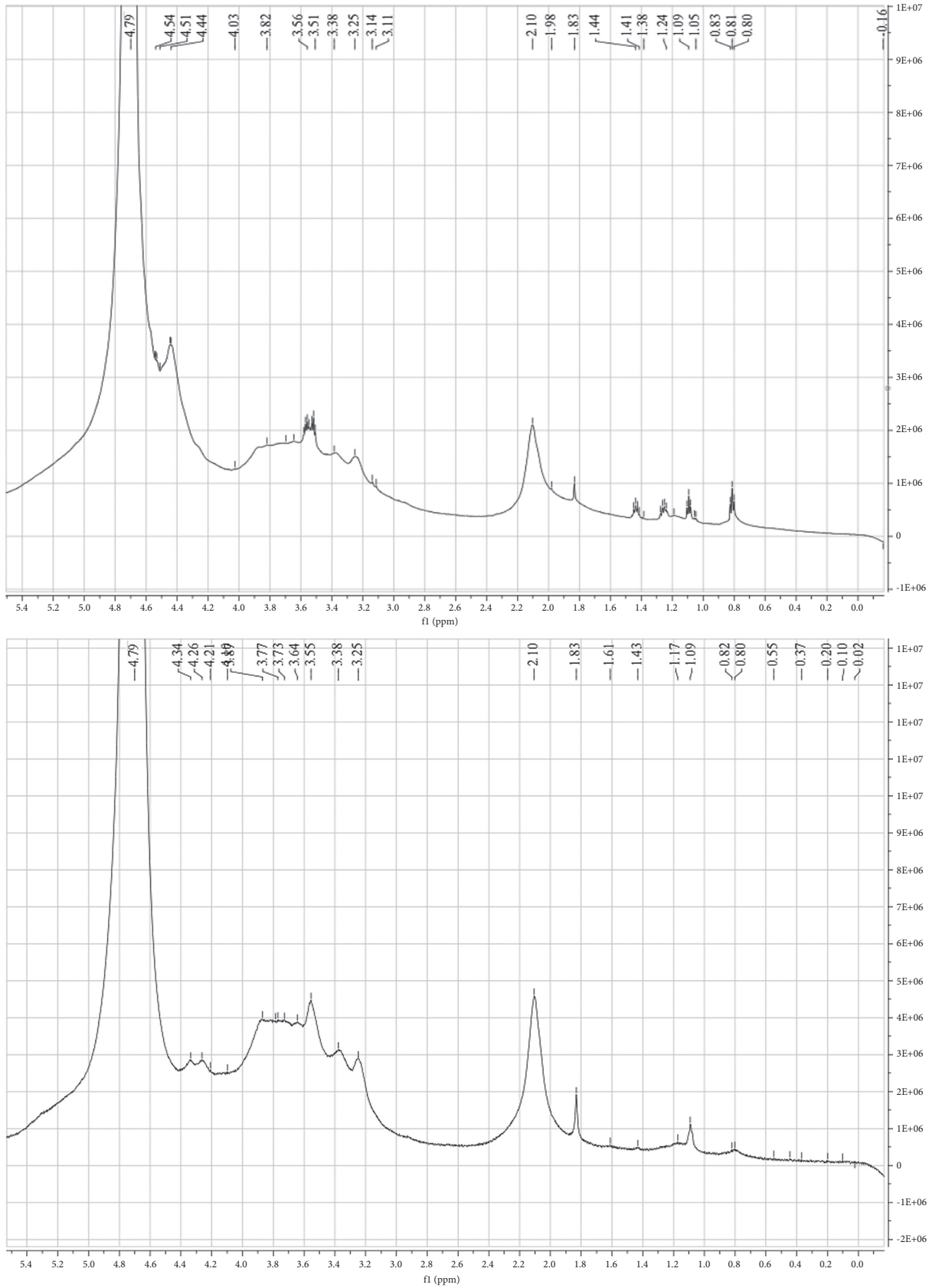

(a)

Figure 6: Continued.

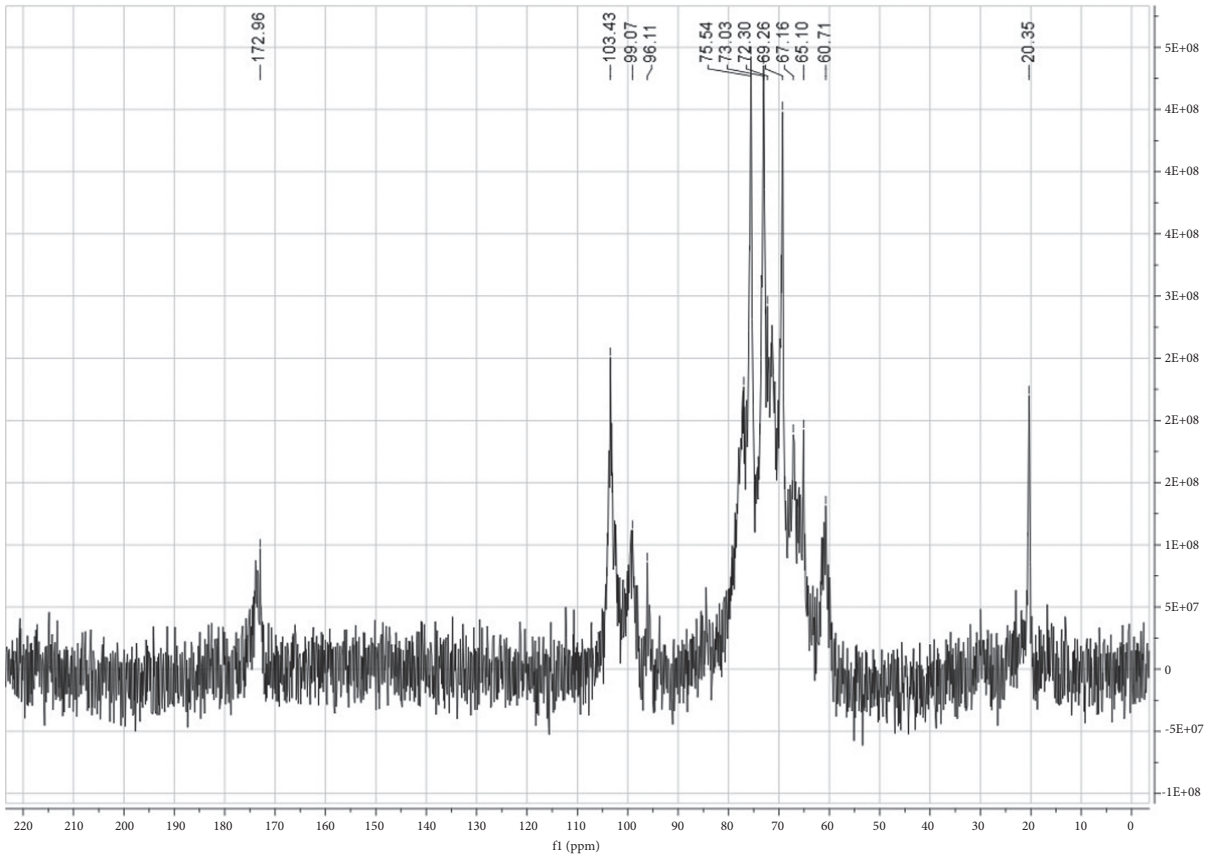

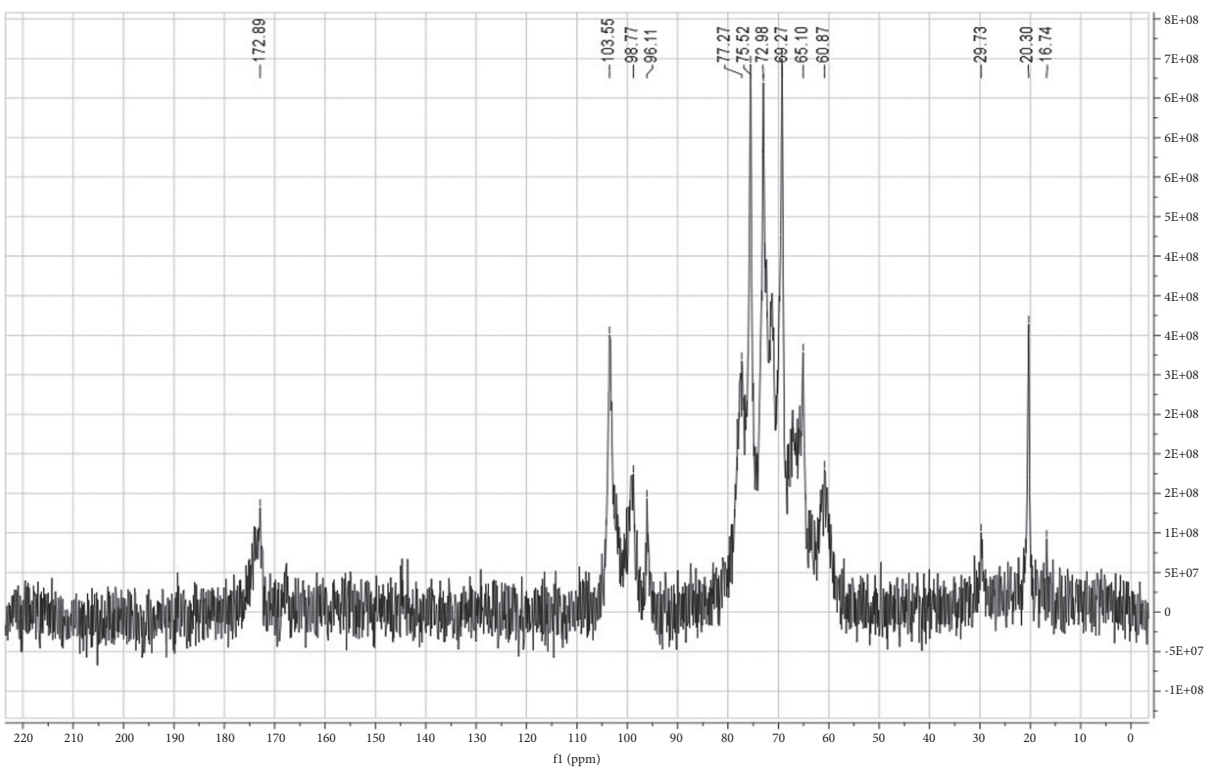

(b)

Figure 6: (a) ^{1}H and (b) ^{13}C NMR spectra of ACEP and the ACEP-Zn complex.

was the signal peak spectrum formed by C_6. After the complex reaction between ACEP and Zn, the signal peak (C_6) located at 67.16 ppm disappeared. All the above-mentioned results indicated that the complex reaction between ACEP and zinc occurred, and the measured results were consistent with the results of FT-IR and ^{1}HNMR.

3.8. Inhibitory Activities against α-Glucosidase

3.8.1. Inhibitory Activities against α-Glucosidase. As shown in Figure 7, ACEP and ACEP-Zn sample solutions had a certain inhibitory effect on α-glucosidase, and the inhibition rate of both increased significantly with the increase of concentration. At the same concentration, the inhibition rate of ACEP-Zn was significantly or extremely significantly greater than that of ACEP. When the concentration was 25 mg/mL, the inhibition rates of ACEP and ACEP-Zn on α-glucosidase both reached the maximum, which were (37.37 ± 0.02)% and (53.74 ± 0.07)%, respectively. After calculation, the half-maximal inhibitory concentration (IC_{50}) of the two inhibitors of α-glucosidase is 34.70 and 21.03 mg/mL, respectively. The smaller the IC_{50}, the stronger the inhibitory ability [36]. It could be seen that the inhibitory ability of ACEP-Zn was stronger than that of ACEP. It can be seen that under the same conditions, the inhibitory ability of ACEP-Zn on α-amylase reached 1.55 times that of ACEP.

3.8.2. Inhibitory Activities against α-Amylase. It could be seen from Figure 8 that at the same concentration, the inhibition rate of ACEP-Zn was extremely significantly greater than that of ACEP. The inhibition rates of ACEP and ACEP-Zn on α-amylase both reached the maximum at the concentration of 25 mg/mL, which were (59.70 ± 1.20)% and (70.47 ± 0.73)%, respectively. After calculation, the IC_{50} of the two inhibiting α-amylases was 17.29 and 11.64 mg/mL, respectively. It could be seen that the inhibitory ability of ACEP-Zn was stronger than that of ACEP.

3.9. Hypoglycemic Activity of ACEP and ACEP-Zn In Vitro

3.9.1. Effect of ACEP-Zn on the Viability of HepG2 Cells. As shown in Figure 9, with the increase of ACEP-Zn concentration, HepG2 cell viability gradually decreased, and the two showed a dose-effect relationship. When the concentration of ACEP-Zn was 10, 25, 50, 100, and 200 μg/mL, the cell viability was (99.85 ± 1.04)%, (96.24 ± 1.77)%, (94.34 ± 0.68)%, (93.29 ± 0.25)%, and (92.90 ± 0.43)%. All were more than 90%, indicating no effect on cell viability. When the concentration of ACEP-Zn was 400 μg/mL, the cell viability was (85.86 ± 1.82)%, indicating that a high concentration of ACEP-Zn has a certain toxic effect on cells. Therefore, in order to eliminate the influence of ACEP-Zn on the viability of HepG2 cells, the concentrations of 10, 25, 50, 100, and 200 μg/mL were selected as the safe administration range, and follow-up experiments were carried out.

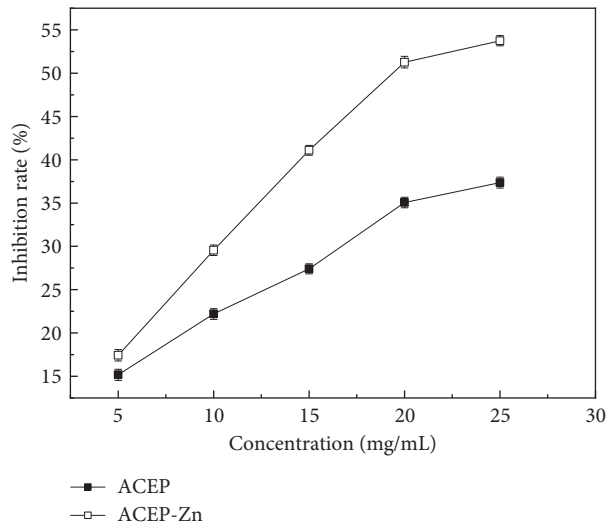

Figure 7: Inhibition rates of α-glucosidase activity.

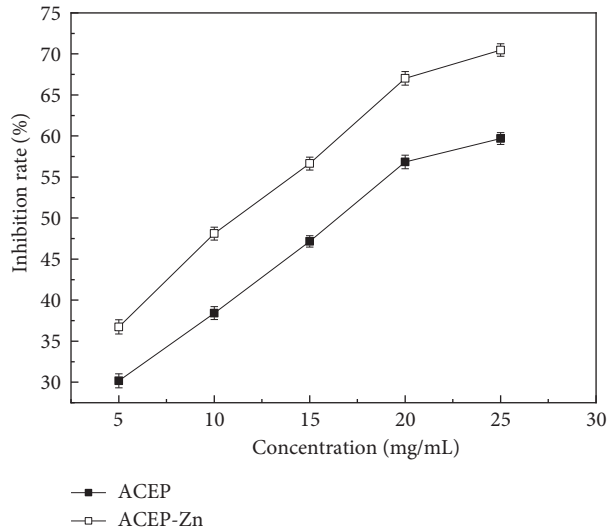

Figure 8: Inhibition rates of α-amylase activity.

3.9.2. Effect of ACEP-Zn on Glucose Consumption of HepG2 Cells. Glucose in the medium mainly supplies the survival and expansion of hepatocytes in vitro. Therefore, the measurement of glucose consumption in cells is the most effective indicator to assess the improvement of IR in different groups. As shown in Figure 10, the cells were treated with 1×10^{-6} concentrations of insulin for 48h. With the normal group, the glucose consumption was obviously decreased comparitively ($P < 0.01$), demonstrating that the insulin resistance model (IR-HepG2 cells) was established successfully. To evaluate the effect of the polysaccharide complex ACEP-Zn on glucose consumption, IR-HepG2 cells were cultivated with different concentrations of ACEP-Zn (10, 25, 50, 100, and 200 μg/mL). ACEP-Zn significantly improved glucose uptake in IR-HepG2 cells compared with the model group. ACEP-Zn (50, 100, and 200 μg/mL) treatment groups can significantly improve its activity ($P < 0.01$, $P < 0.05$). At a concentration of 100 μg/mL,

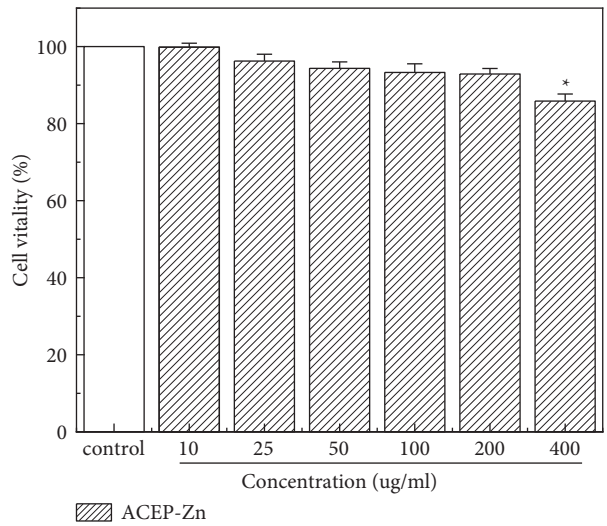

Figure 9: The effect of peptide LPLLR on HepG2 cells viability. Data are presented as mean ± SD ($n = 5$). $^{*}P < 0.05$ vs. the model group.

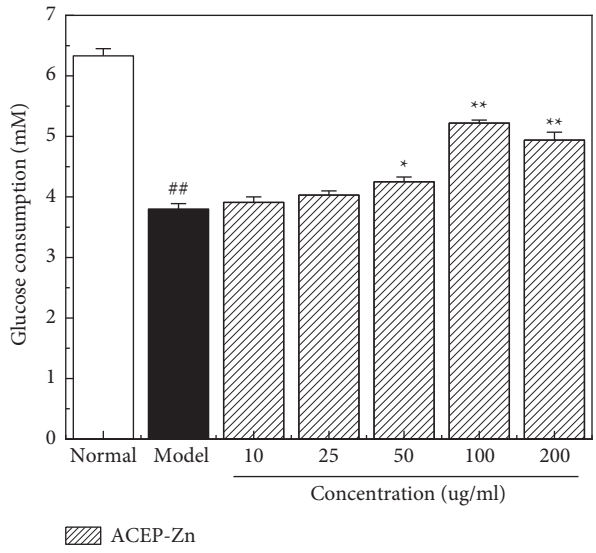

Figure 10: The effect of ACEP and the ACEP-Zn complex on glucose consumption in IR-HepG2 cells. Data are expressed as average ± SD ($n = 5$). $^{\#}P < 0.05$, $^{\#\#}P < 0.01$ vs. the nomal group; $^{*}P < 0.05$, $^{**}P < 0.05$ vs. the model group.

ACEP-Zn showed a significant increase in glucose consumption in HepG2 cells, which was comparable to that in the normal group. Therefore, it indicated that the polysaccharide complex ACEP-Zn could improve glucose consumption in IR-HepG2 cells. The result is similar to the study of Wang and others.

3.9.3. Determination of Activities of SOD and NOS. The emergence and development of diabetes lead to the increase of free radicals and the decrease of antioxidant capacity, which leads to the emergence of an oxidative stress response. Oxidative stress leads to apoptosis, hyperglycemia, hyperinsulinemia, and dyslipidemia and plays an important role in diabetes and diabetes-related complications [37]. Some hypoglycemic drugs can reduce oxidative stress in cells. Therefore, we also measured the activities of SOD and NOS in HepG2-IR cells, and the results are shown in Figures 11(a) and 11(b). The SOD activity in the model group was significantly lower than that in the normal group ($P < 0.01$). Compared with the model group, the SOD activity of the experimental group (ACEP-Zn) was increased in a concentration-dependent manner, suggesting that ACEP-Zn can significantly reduce the oxidative stress of HepG2-IR cells, which is closely connected with the regulation of IR.

In addition, the NOS activity of the model group was significantly higher than that of the normal group. Compared with the normal group, NOS activity was significantly increased in the insulin resistance model group ($P < 0.01$). Compared with the insulin resistance model group, the addition of ACEP-5-Zn at different concentrations (10, 25, 50, 100, and 200 μg/mL) significantly reduced the intracellular NOS activity, and the difference was statistically significant ($P < 0.05$, $P < 0.01$) and decreased with the increase of ACEP-Zn concentration, showing a certain dose-dependent relationship.

3.9.4. Determination of Activities of PK. PK is a key rate-limiting enzyme in the glycolytic pathway, whose main function is to convert phosphoenolpyruvate and ADP into ATP and pyruvate, which also plays an important role in liver glucose uptake and glucose regulation [38]. The experiment was conducted by PK. To evaluate the effect of ACEP-Zn on the glucose metabolism of IR-HepG2 cells (Figure 12). Compared with the model group, the PK activity of ACEP-Zn groups was significantly increased ($P < 0.05$, $P < 0.01$). When the concentration of ACEP-Zn reached 200 μg/mL, the activity of HK was close to that of the normal group. In conclusion, ACEP-Zn has a significant effect on glucose metabolism by regulating the activities of key-related enzymes.

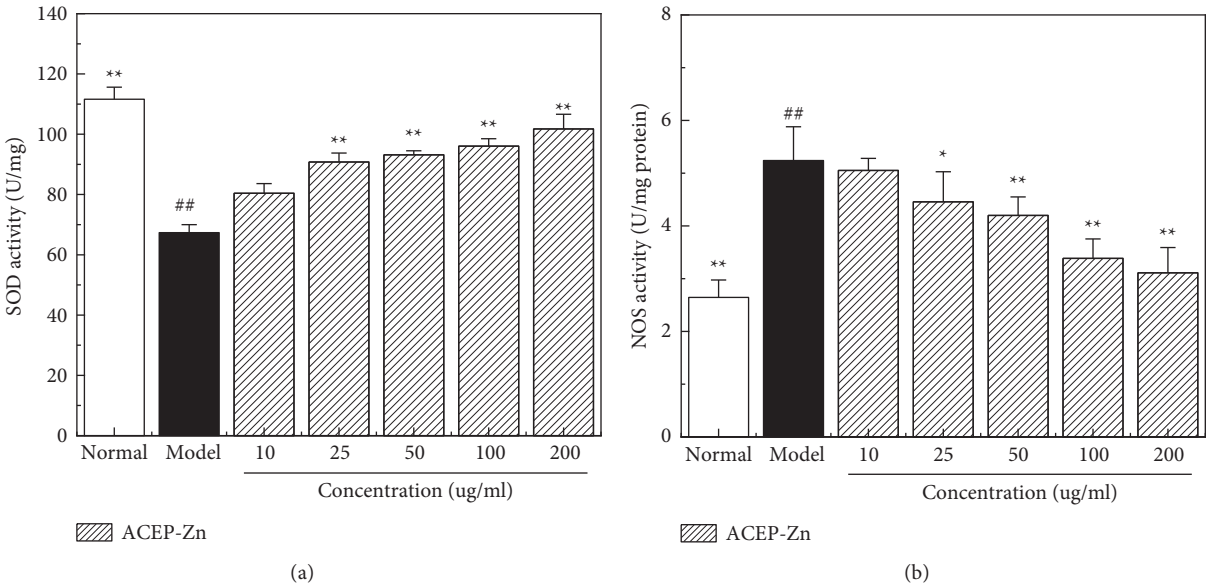

Figure 11: The effects of ACEP and the ACEP-Zn complex on (a) the activities of SOD and (b) NOS in IR-HepG2 cells. Data are expressed as average ± SD ($n = 5$). $^{\#}P < 0.05$, $^{\#\#}P < 0.01$ vs. the nomal group; $^{*}P < 0.01$, $^{**}P < 0.05$ vs. the model group.

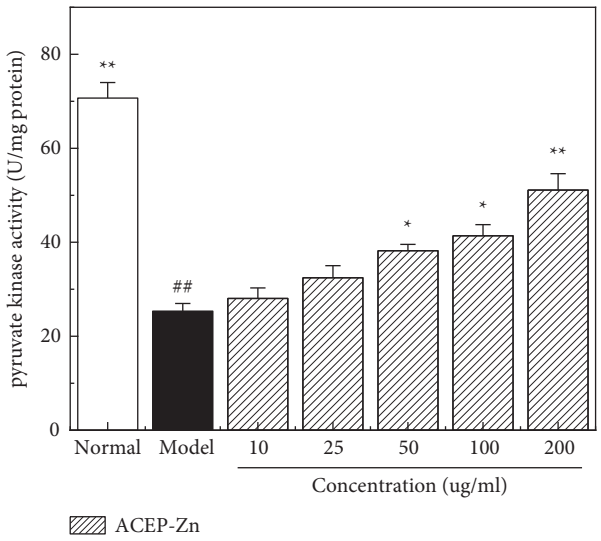

Figure 12: The effects of ACEP and the ACEP-Zn complex on the activities of PK in IR-HepG2 cells. Data are presented as mean ± SD ($n = 5$). $^{\#}P < 0.05$, $^{\#\#}P < 0.01$ vs. the nomal group; $^{*}P < 0.05$, $^{**}P < 0.01$ vs. the model group.

4. Conclusion

In this study, we used FT-IR, XRD, SEM, and NMR to characterize polysaccharide and its Zn^{2+} complex structure characterization and evaluate their hypoglycemic activity in vitro. The results indicated that the structure of *Auricularia auricula* polysaccharide was changed obviously after zinc complex, and its hypoglycemic activity was enhanced in vitro. In the cell experiment, the glucose consumption of IR-HepG2 cells was significantly increased at a concentration of 50–200 μg/mL ($P < 0.05$). The activities of SOD and NOS increased ($P < 0.01$). The activity of intracellular PK increased ($P < 0.05$). In conclusion, the molecular structure characteristics of *Auricularia cornea Ehrenb* Zn^{2+} were significantly changed compared with the original polysaccharide, and the hypoglycemic activity of the *Auricularia cornea Ehrenb* polysaccharide Zn^{2+} complex was significantly enhanced in vitro. As a new kind of polysaccharide Zn^{2+} supplement, *Auricularia cornea Ehrenb* polysaccharide Zn^{2+} complex has broad development prospects.

Data Availability

The data used to support the findings of this study are available from the corresponding author upon request.

Conflicts of Interest

All authors declare that there are no conflicts of interest.

Authors' Contributions

All authors read and approved the final manuscript.

Acknowledgments

This study was financially supported by the Key Projects of the National Research and Development Program of China (Grant no. 2018YFD0400204).

References

[1] P. Saeedi, I. Petersohn, P. Salpea et al., "Global and regional diabetes prevalence estimates for 2019 and projections for 2030 and 2045: results from the international diabetes federation diabetes atlas, 9th edition," *Diabetes Research and Clinical Practice*, vol. 157, p. 107843, 2019.

[2] E. Krishnan, B. J. Pandya, L. Chung, A. Hariri, and O. Dabbous, "Hyperuricemia in young adults and risk of

insulin resistance, prediabetes, and diabetes: a 15-year follow-up study," *American Journal of Epidemiology*, vol. 176, no. 2, pp. 108–116, 2012.

[3] G. Liu, L. Liang, G. Yu, and Q. Li, "Pumpkin polysaccharide modifies the gut microbiota during alleviation of type 2 diabetes in rats," *International Journal of Biological Macromolecules*, vol. 115, pp. 711–717, 2018.

[4] D. M. Muoio and C. B. Newgard, "Molecular and metabolic mechanisms of insulin resistance and β-cell failure in type 2 diabetes," *Nature Reviews Molecular Cell Biology*, vol. 9, no. 3, pp. 193–205, 2008.

[5] S. E. Kahn, R. L. Hull, and K. M. Utzschneider, "Mechanisms linking obesity to insulin resistance and type 2 diabetes," *Nature*, vol. 444, no. 7121, pp. 840–846, 2006.

[6] D. Patel, R. Kumar, D. Laloo, and S. Hemalatha, "Natural medicines from plant source used for therapy of diabetes mellitus: an overview of its pharmacological aspects," *Asian Pacific Journal of Tropical Disease*, vol. 2, no. 3, pp. 239–250, 2012.

[7] A. S. Prasad, "Zinc: an overview," *Nutrition*, vol. 11, pp. 93–99, 1995.

[8] S. F. Simon and C. G. Taylor, "Dietary zinc supplementation attenuates hyperglycemia in db/db mice," *Experimental Biology and Medicine*, vol. 226, no. 1, pp. 43–51, 2001.

[9] L. G. Søndergaard, M. Stoltenberg, and P. Doering, "Zinc ions in the endocrine and exocrine pancreas of zinc deficient rats," *Histology & Histopathology*, vol. 21, no. 6, pp. 619–625, 2006.

[10] Y. Yoshikawa, A. Murayama, and Y. Adachi, "Challenge of studies on the development of new Zn complexes (Zn(opt)2) to treat diabetes mellitus," *Metall*, vol. 3, pp. 686–692, 2011.

[11] W. Basuki, M. Hiromura, and H. Sakurai, "Insulinomimetic Zn complex (Zn(opt)2) enhances insulin signaling pathway in 3T3-L1 adipocytes," *Journal of Inorganic Biochemistry*, vol. 101, no. 4, pp. 692–699, 2007.

[12] E. S. Eshak, H. Iso, K. Maruyama, I. Muraki, and A. Tamakoshi, "Associations between dietary intakes of iron, copper and zinc with risk of type 2 diabetes mellitus: a large population-based prospective cohort study," *Clinical Nutrition*, vol. 37, no. 2, pp. 667–674, 2018.

[13] N. Xu, Z. Ren, J. Zhang et al., "Antioxidant and anti-hyperlipidemic effects of mycelia zinc polysaccharides by Pleurotus eryngii var.Tuoliensis," *International Journal of Biological Macromolecules*, vol. 95, pp. 204–214, 2017.

[14] C. Zhang, Z. Gao, C. Hu et al., "Antioxidant, antibacterial and anti-aging activities of intracellular zinc polysaccharides from Grifola frondosa SH 05," *International Journal of Biological Macromolecules*, vol. 95, pp. 778–787, 2017.

[15] Y. C. Cao, H. Y. Bao, X. Li, B. Tolgor, and Y. Li, "Anti-tumor activities of Auricularia cornea fruiting body ecjxtract in H-(22) bearing mice," *Mycosystema*, vol. 36, p. 10, 2017.

[16] Y. R. Zhang, D. W. Wang, and Y. T. Chen, "Healthy function and high valued utilization of edible fungi," *Food Science and Human Wellness*, vol. 10, no. 4, pp. 408–420, 2021.

[17] C. Zyab, C. Zlab, C. Clab, C. Jwab, C. Cmab, and C. Wkab, "Immunomodulatory effects of polysaccharides from edible fungus: a review," *Food Science and Human Wellness*, vol. 10, no. 4, pp. 393–400, 2021.

[18] D. Wang, X. Jiang, S. Teng, Y. Zang, and Y. Li, "The antidiabetic and antinephritic activities of auricularia cornea (an albino mutant strain) via modulation of oxidative stress in the db/db mice," *Frontiers in Immunology*, vol. 1039, 2019.

[19] F. S. Jing, *Optimization of Extraction Process of Polysaccharides from Auricularia Auricularia and Development of Anti-fatigue Milk Beverage from Auricularia Auricularia*, Jilin Agricultural University, Changchun, China, 2016.

[20] G. Qin, W. Xu, J. Liu, L. Zhao, and G. Chen, "Purification, characterization and hypoglycemic activity of glycoproteins obtained from pea (pisum sativum l.)," *Food Science and Human Wellness*, vol. 10, no. 3, pp. 297–307, 2021.

[21] S. A. Adefegha, G. Oboh, and O. S. Omojokun, "In vitro antioxidant activities of African birch (Anogeissus leiocarpus) leaf and its effect on the α-amylase and α-glucosidase inhibitory properties of acarbose," *Journal of Taibah University Medical Sciences*, vol. 11, no. 3, pp. 236–242, 2016.

[22] J. Wang, T. Wu, and L. Fang, "Anti-diabetic effect by walnut (Juglans mandshurica Maxim.)-derived peptide LPLLR through inhibiting α-glucosidase and α-amylase, and alleviating insulin resistance of hepatic HepG2 cells," *Journal of Functional Foods*, vol. 69, p. 103944, 2020.

[23] M. Zang, A. Zuccollo, and X. Hou, "AMP-activated protein kinase is required for the lipid-lowering effect of metformin inresistant human HepG2 cells," *Journal of Biological Chemistry*, vol. 279, pp. 47898–47905, 2004.

[24] Y. L. Hao, H. Q. Sun, and X. J. Zhang, "A novel acid polysaccharide from fermented broth of Pleurotus citrinopileatus: hypoglycemic activity in vitro and chemical structure," *Journal of Molecular Structure*, vol. 1220, p. 128717, 2020.

[25] Y. Koike, K. Hagiwara, and T. Nakamura, "Enhancement of the atomic absorbance of Cr, Zn, Cd, and Pb in metal furnace atomic absorption spectrometry using absorption tubes," *Analytical Chemistry*, vol. 11, pp. 9–12, 2017.

[26] D. F. Wen, T. Chen, and M. F. Yan, "Synthesis, characterization, antioxidant activity and neuroprotective effects of selenium polysaccharide from Radix hedysari," *Carbohydrate Polymers*, vol. 125, pp. 161–168, 2015.

[27] P. P. Wang, Q. Huang, and C. Chen, "The chemical structure and biological activities of a novel polysaccharide obtained from Fructus Mori and its zinc derivative," *Journal of Functional Foods*, vol. 54, pp. 64–73, 2019.

[28] Z. Luo, "Nie preparation and properties of enzyme-modified cassava starch–zinc complexes," *Journal of Agricultural and Food Chemistry*, vol. 61, no. 19, pp. 4631–4638, 2013.

[29] Y. Chi, Y. Li, and G. Zhang, "Effect of extraction techniques on properties of polysaccharides from Enteromorpha prolifera and their applicability in iron chelation," *Carbohydrate Polymers*, vol. 181, pp. 616–623, 2018.

[30] C. Ou, S. Chen, Y. Liu, J. Shao, S. Li, and T. Fu, "Study on the thermal degradation kinetics and pyrolysis characteristics of chitosan-Zn complex," *Journal of Analytical and Applied Pyrolysis*, vol. 122, pp. 268–276, 2016.

[31] Z. A. Yun, C. Khan, and A. Yuan, "Preparation and characterization of D. opposita Thunb polysaccharide-zinc inclusion complex and evaluation of anti-diabetic activities," *International Journal of Biological Macromolecules*, vol. 121, pp. 1029–1036, 2019.

[32] M. M. Corsaro, C. D. Castro, and T. Naldi, "1H and 13C NMR characterization and secondary structure of the K2 polysaccharide of *Klebsiella pneumoniae* strain 52145," *Carbohydrate Research*, vol. 340, pp. 2212–2217, 2005.

[33] W. Liu, X. Lv, W. Huang, W. Yao, and X. Gao, "Characterization and hypoglycemic effect of a neutral polysaccharide extracted from the residue of Codonopsis Pilosula," *Carbohydrate Polymers*, vol. 197, pp. 215–226, 2018.

[34] H. Yao, J. Q. Wang, and J. Y. Yin, "A review of nmr analysis in polysaccharide structure and conformation: progress, challenge and perspective," *Food Research International*, vol. 143, p. 110290, 2021.

[35] J. Chen, X. Zhang, and D. Huo, "Preliminary characterization, antioxidant and α-glucosidase inhibitory activities of polysaccharides from Mallotus furetianus," *Carbohydrate Polymers*, vol. 215, pp. 307–315, 2019.

[36] J. J. Zhang, L. Zhou, and L. L. Cui, "Antioxidant and -glucosidase inhibitiory activity of Cercis chinensis flowers," *Food Science and Human Wellness*, vol. 9, pp. 313–319, 2020.

[37] M. Y. Ali, S. Zaib, and M. M. Rahman, "Didynni, a dietary citus flavonoid exlibit anti-diabetioconplicatioit and promotes ghcose uptake tluough the activation of PI3K/Akt sigialig patlw ay ininuulin-1esittant HepG2 cell," *Chemico-Biological Interactions*, vol. 305, pp. 180–194, 2019.

[38] K. Zhu, S. Nie, and L. Tan, "A polysaccharide from ganoderma atrum improves liver function in type 2 diabetic rats via antioxidant action and short-chain fatty acids excretion," *Journal of Agricultural and Food Chemistry*, vol. 64, no. 9, pp. 1938–1944, 2016.